Supplementary Information for

A theoretical study of wrinkle propagation in graphene with flower-like grain boundaries

Zihui Zhao [a, b, 1], Yafei Wang [a, b, 1], Changguo Wang [a, b, *]

[a] National Key Laboratory of Science and Technology on Advanced Composites in Special Environments, Harbin Institute of Technology, Harbin 150001, PR China

[b] Center for Composite Materials and Structures, Harbin Institute of Technology, Harbin 150001, PR China

[*] Corresponding author, E-mail addresses: wangcg@hit.edu.cn (C. Wang).

[1] These authors contributed equally to this work.

This supplementary information material contains details of theoretical analysis and atomistic simulations for wrinkle propagation in graphene with flower-like rotational grain boundaries (GBs).

Content:

Note 1. Experimental scanning tunnel microscope (STM) topographic images of the rotational GB

Note 2. Simulation methodology

Note 3. Evolution of the instantaneous atomic kinetic and strain energies for pristine graphene

Note 4. Continuum model and contact law for the C60 molecule and pristine graphene

Note 5. Polar coordinate system and specific atomic positions in graphene sheets

Note 6. Variations of specific atomic x- and y-coordinate for atoms in the $(r,\pi/4)$ axis

Note 7. Variations of specific atomic strain energy for atoms in the $(r,\pi/4)$ axis

Note 8. Evolution of van der Waals (vdW) potential energy for the graphene sheets

Note 9. Effects of initial velocity and temperature variation on the out-of-plane displacement along the $(r,0)$ and $(r,\pi/2)$ axes

Note 10. Wrinkle propagation in the graphene sheets with point and Stone Wales (SW) defects

Note 11. Evolution of various energies for the graphene sheets with external excitation

Note 12. Out-of-plane displacements of the graphene sheets at different time with external excitation

Note 1. Experimental scanning tunnel microscope (STM) topographic images of the rotational GB

Fig. S1 shows the experimental STM topographic images of the rotational GB from Ref.[1].
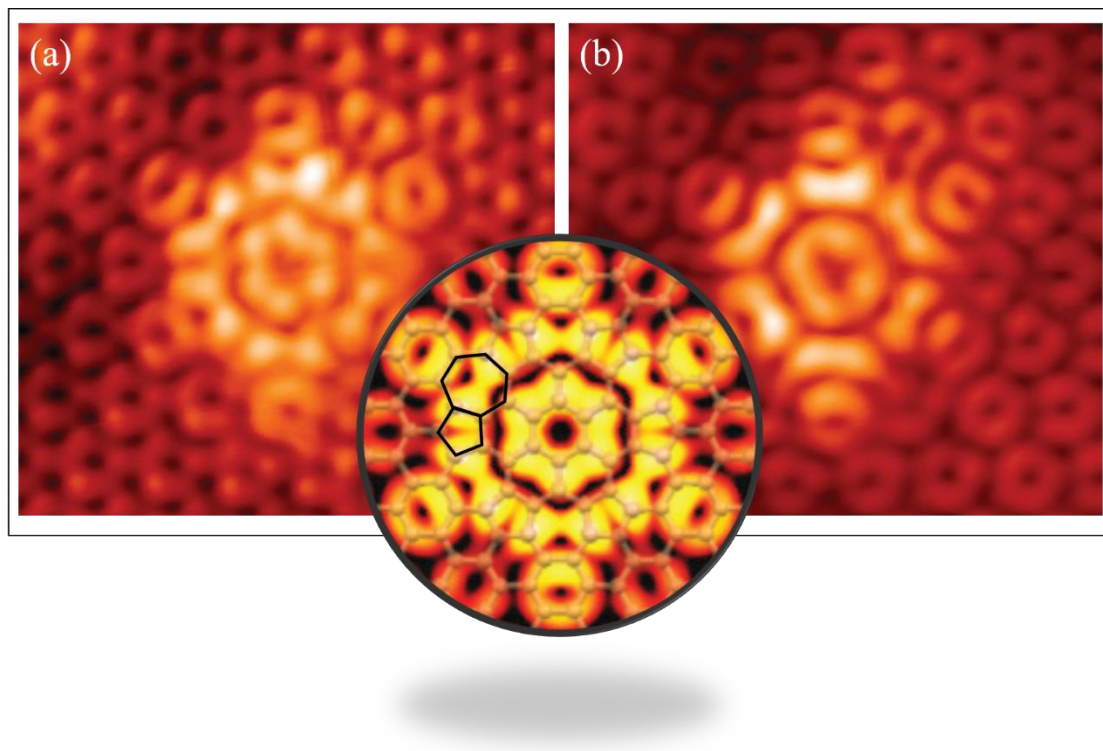

Fig. S1. Experimental STM topographic images of the rotational GB from Ref.[1]. STM topographic images of rotational GB observed in the growth of epitaxial graphene on SiC at (a) -300 mV and (b) 300 eV sample bias. The color gradation for carbon atoms is from dark to bright according to their topographic height variations of (a) 150 pm and (b) 130 pm.

Note 2. Simulation methodology

The potential energy stored in the C60-graphene system can be directly expressed as:

$$E_{Total} = E^{AIREBO} = \frac{1}{2} \sum_i \sum_{j \neq i} \left(E_{ij}^{LJ} + \sum_{k \neq i,j} \sum_{l \neq i,j,k} E_{kijl}^{tors} + E_{ij}^{REBO} \right) \tag{1}$$

where, the AIREBO potential[2] consists of three sub-potentials: the standard long-range two-body Lennard-Jones (L-J) potential, the 4-body torsional interaction potential and the Reactive Empirical Bond-Order (REBO) potential. E_{ij}^{LJ}, E_{kijl}^{tors} and E_{ij}^{REBO} are respectively the 12-6 L-J potential, the torsional potential and REBO potential[3]. The 12-6 L-J potential can be calculated using the following relationship:

$$E_{ij}^{LJ} = 4\varepsilon \left[\left(\frac{\sigma_{ij}}{r_{ij}} \right)^{12} - \left(\frac{\sigma_{ij}}{r_{ij}} \right)^6 \right] \tag{2}$$

where ε is the energy scale parameter and σ is the collision diameter parameter[4] in current research. r_{ij} is the distance between atom i and atom j. The torsional potential is implemented in AIREBO for all dihedral angles in the system[2]:

$$E_{kijl}^{tors} = \frac{1}{2} \sum_i \sum_{j \neq i} \sum_{k \neq i,j} \sum_{l \neq i,j,k} w_{ij}\left(r_{ij}\right) w_{jk}\left(r_{jk}\right) w_{kl}\left(r_{kl}\right) \times V^{tors}\left(\omega_{ijkl}\right) \tag{3}$$

where $w(r)$ is the bond weight (the value is between 0 to 1), that is used as an indication of the bonding between atoms. $V^{tors}(\omega)$ is the torsional potential with a single minimum, and it can be given in terms of a cosine power series in the dihedral angle ω:

$$V^{tors} = \frac{256}{405} \varepsilon_{kijl} cos^{10}\left(\frac{\omega_{kijl}}{2} \right) - \frac{1}{10} \varepsilon_{kijl} \tag{4}$$

The REBO potential energy functional is adapted from Ref.[5], it can be written as follows:

$$E_{ij}^{REBO} = V_{ij}^R + b_{ij} V_{ij}^A \tag{5}$$

where b_{ij} is the bond order, it represents the pairwise interaction strength. Depending

on bond bending, dihedral angles and the radical character of the bond[6], the bond order can be determined as:

$$b_{ij} = \frac{1}{2}\left(p_{ij}^{\sigma\pi} + p_{ji}^{\sigma\pi} \right) + \pi_{ij}^{rc} + \pi_{ij}^{dh} \tag{6}$$

As to repulsive term:

$$V_{ij}^{R} = w_{ij}\left(r_{ij}\right)\left(1 + \frac{Q_{ij}}{r_{ij}}\right)A_{ij}e^{-\alpha_{ij}r_{ij}} \tag{7}$$

where the parameters $Q_{ij} = 0.313460$ Å, $A_{ij} = 10953.544$ eV and $\alpha_{ij} = 4.7465391$ Å^{-1} in current system. As to attractive term:

$$V_{ij}^{A} = -w_{ij}\left(r_{ij}\right)\sum_{n=1}^{3} B_{ij}^{(n)}e^{-\beta_{ij}^{(n)}r_{ij}} \tag{8}$$

where the parameters $B_{ij}^{(1)}$, $B_{ij}^{(2)}$ and $B_{ij}^{(3)}$ are 12388.792 eV, 17.567065 eV and 30.714932 eV, respectively. The parameters $\beta_{ij}^{(1)}$, $\beta_{ij}^{(2)}$ and $\beta_{ij}^{(3)}$ are 4.7204523 Å^{-1}, 1.4332132 Å^{-1} and 1.3826913 Å^{-1}, respectively.

Note 3. Evolution of the instantaneous atomic kinetic and strain energies for pristine graphene

Figs. S2a-b reveal the evolutions of instantaneous atomic kinetic and strain energies for pristine graphene over time. With time increasing, the circular contours for the evolution of the kinetic energy (see 750 fs-1750 fs in **Fig. S2**a) and the significant reflection for the strain energy (after 1000 fs in **Fig. S2**b) can be observed.
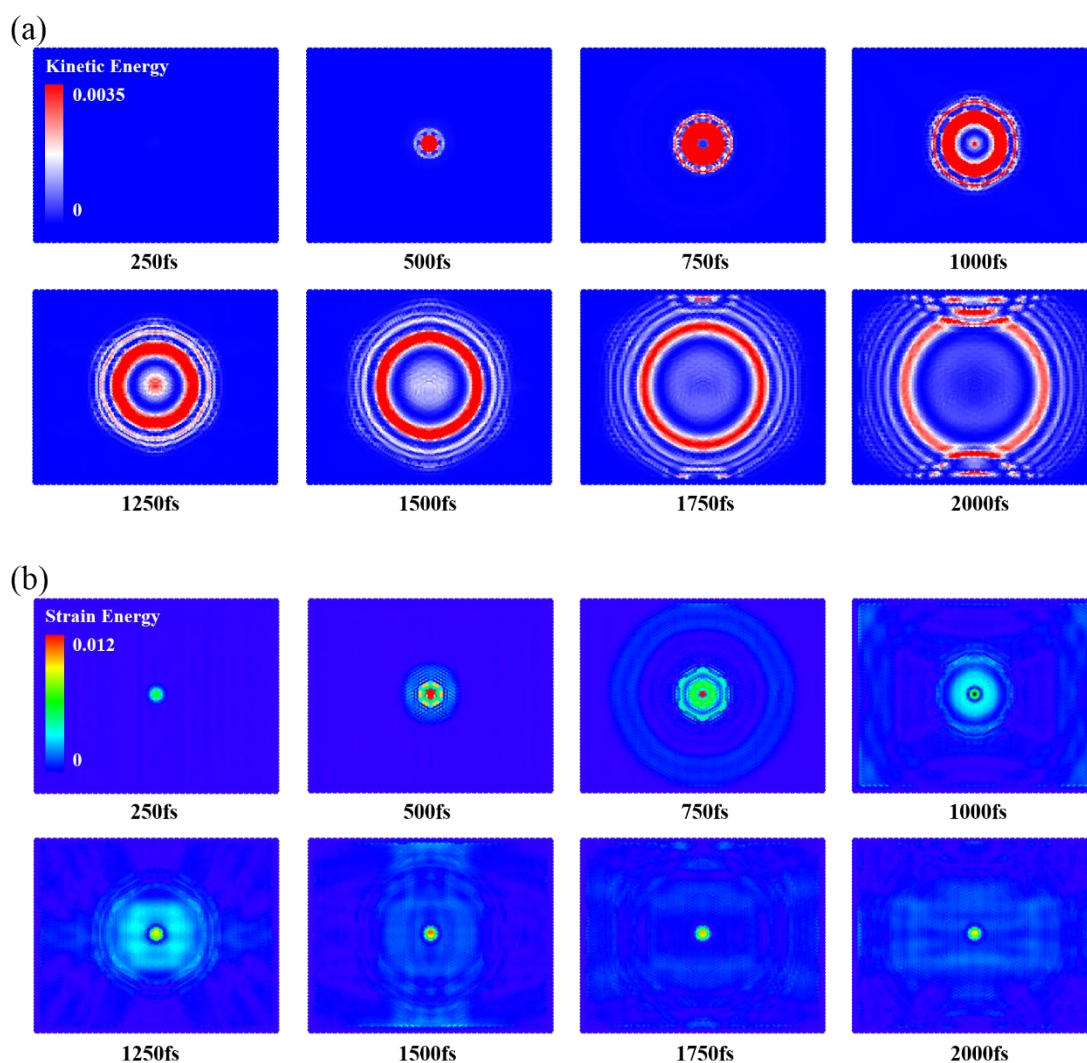
(a)

(b)

Fig. S2. Energy evolution in pristine graphene motivated by C60 molecule. Atomic snapshots are from 250fs to 2000fs, with a time span of 250 fs. (a) The distribution of the instantaneous atomic kinetic energy in units of eV. Atoms are colour coded with blue mapped to the lowest value. (b) The distribution of the instantaneous atomic strain energy in units of eV. Atoms are colour coded with red mapped to the highest value.

Note 4. Continuum model and contact law for the C60 molecule and pristine graphene

The schematic diagram for the C60-C$_6$(0) (i.e., pristine graphene) system is illustrated in **Fig. S3**. In the following, the contact law based on continuum mechanics[7-9] is used to study the nanoscale interactions. The molecular interaction between the C60 molecule and pristine graphene is modeled by the classical 12-6 Lenard-Jones (L-J) potential[10]:

$$E_{L-J} = 4\varepsilon \left[\left(\frac{\sigma}{l} \right)^{12} - \left(\frac{\sigma}{l} \right)^{6} \right] \tag{9}$$

where l, $\varepsilon = 2.864 \, \text{meV}$ and $\sigma = 0.347 \, \text{nm}$ denote the atomic distance of two atoms, the potential well depth between two arbitrary atoms and the L-J distance, respectively[11]. As shown in **Fig. S3**a, the C60-C$_6$(0) contact system is modeled by using a hollow-ball as the C60 molecule and an infinite plate as pristine graphene. In addition, $R - \phi - \theta$ spherical coordinate system for the hollow-ball and $r - \psi$ polar coordinate system for the plate are constructed, respectively. Thus, the L-J potential for two elements (see **Fig. S3**a) can be stated as:

$$dE_{L-J} = 4 p q \varepsilon R^2 \left[\frac{\sigma^{12}}{\left(H'^{\,2} + r^2 \right)^6} - \frac{\sigma^6}{\left(H'^{\,2} + r^2 \right)^3} \right] \sin\theta \, d\theta \, d\phi \, r \, dr \, d\psi \tag{10}$$

where $p = 60/\left(4\pi R^2 \right)$ and $q = 4/\left(3\sqrt{3} L_{C-C}^2 \right)$ ($L_{C-C} = 0.142 \, \text{nm}$ in Ref.[10]) are the number of particles per unit area of C60 and the number of particles per unit area of pristine graphene, respectively[8]. As shown in **Fig. S3**a, θ, ϕ, R, r and ψ stand for the coordinate parameters for the spherical coordinate system of the hollow-ball and the polar coordinate system of the plate, respectively. The L-J potential can be obtained by integrating Eq. (10):

$$\int_{\psi=0}^{2\pi} \int_{r=0}^{\infty} dE_{L-J} = \pi p q \varepsilon R^2 \sin\theta \, d\theta \, d\phi \left[\frac{4\sigma^{12}}{5 H'^{\,10}} - \frac{2\sigma^6}{H'^{\,4}} \right] \tag{11}$$

Based on the geometric relationship in **Fig. S3**a, H' can be expressed as $H + R(1 + \cos\theta)$. Then the L-J potential between the hollow-ball and infinite plate is given by:

$$E_{L-J} = \pi^2 pq\varepsilon R \left[\frac{8}{45} \sigma^{12} \left(\frac{1}{H^9} - \frac{1}{(H+2R)^9} \right) \right.$$
$$\left. - \frac{4}{3} \sigma^6 \left(\frac{1}{H^3} - \frac{1}{(H+2R)^3} \right) \right] \tag{12}$$

For the smaller inter-distances compared with R, Eq. (12) can be approximately expressed as:

$$E_{L-J} = \pi^2 pq\varepsilon R \left[\frac{8}{45} \frac{\sigma^{12}}{H^9} - \frac{4}{3} \frac{\sigma^6}{H^3} \right] \tag{13}$$

Correspondingly, the z-direction interaction force, F_z, can be obtained by the derivative of the L-J potential in terms of distance H:

$$F_z = -\frac{\partial E_{L-J}}{\partial H} = 4\pi^2 pq\varepsilon R \left[\frac{2}{5} \frac{\sigma^{12}}{H^{10}} - \frac{\sigma^6}{H^4} \right] \tag{14}$$

For the molecular dynamics (MD) model shown in **Fig. S3**b, pristine graphene is modeled by a plate with the length, width and thickness respectively represented by a, b and h. Based on Kirchhoff's assumptions[9], the motion equation for a nonlocal plate can be given by:

$$I_0 \left(1 - e_0^2 a^2 \nabla^2 \right) \ddot{w} = -D_{xx} w_{0,xxxx} - 2 \left(D_{xy} + D_{ss} \right) w_{0,xxyy}$$
$$- D_{yy} w_{0,yyyy} + \left(1 - e_0^2 a^2 \nabla^2 \right) PR^2 \tag{15}$$

where w is z-direction displacement of the plate, $I_0 = 7.61 \times 10^{-7} \, \text{kg/m}^2$ is the mass momentum of inertia, $D_{xx} = 4.03 \times 10^{-17}$ J, $D_{yy} = 3.97 \times 10^{-17}$ J, $D_{xy} = 2.65 \times 10^{-17}$ J, $D_{ss} = 1.06 \times 10^{-17}$ J are the flexural rigidity and e_0 is non-dimensional nonlocal parameter. Out-of-plane displacement of the plate, w, can be obtained[7]:

$$w(x, y, t) = \sum_{i,j=1}^{\infty} \psi_{ij}(x, y) \eta_{ij}(t) \tag{16}$$

where, $\psi_{ij}(x, y)$ is the mode shapes of vibrations and $\eta_{ij}(t)$ is defined as the time-dependent coefficients for $\psi_{ij}(x, y)$. ij denote the i, j^{th} vibration model. $\psi_{ij}(x, y)$ can be written as:

$$\omega_{ij}^2 = \frac{\pi^4}{a^2 b^2 I_0} \frac{i^4 b^4 D_{xx} + 2i^2 j^2 a^2 b^2 \left(D_{xy} + D_{ss}\right) + j^4 a^4 D_{yy}}{a^2 b^2 + \pi^2 e_0^2 a^2 \left(i^2 b^2 + j^2 a^2\right)}$$

$$\psi_{ij} = \sin\frac{i\pi x}{a} \sin\frac{j\pi y}{b} \quad (i, j = 1, 2, \cdots, \infty) \tag{17}$$

Accordingly, $\eta_{ij}(t)$ can be expressed as:

$$\eta_{ij}(t) = \cos\left(\omega_{ij}t\right)\eta_{ij}(0) + \frac{\sin\left(\omega_{ij}t\right)}{\omega_{ij}}\dot{\eta}_{ij}(0)$$

$$-\frac{C_{ij}}{\omega_{ij}}\int_0^t F_z(\xi)\sin\left[\omega_{ij}(t-\xi)\right]d\xi \tag{18}$$

where $F_z(\xi)$ and C_{ij} are the amplitude of impact force and the influence coefficient of impact loading, respectively. Correspondingly, C_{ij} can be obtained:

$$C_{ij} = \frac{\left(\psi_{ij} - e_0^2 a^2 \psi_{ij,xx} - e_0^2 a^2 \psi_{ij,yy}\right)_{(x_0,y_0)}}{I_0 \int_A \psi_{ij}\left(1 - e_0^2 a^2 \nabla^2\right)\psi_{ij}dA} \tag{19}$$
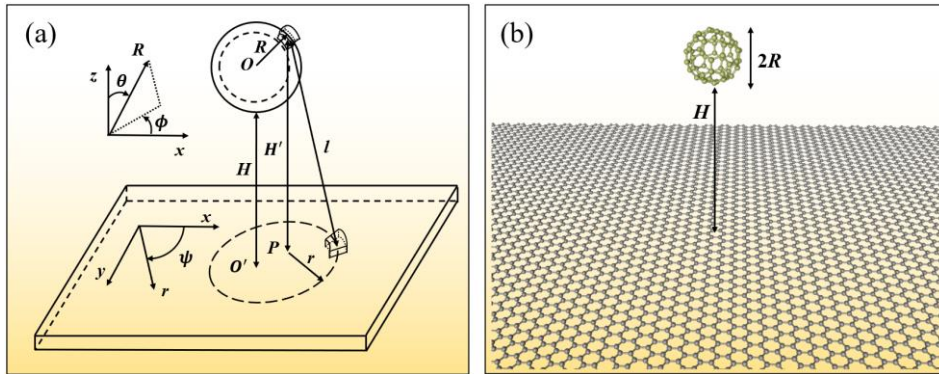
Fig. S3. Schematic illustration of C60-C6(0) (i.e., pristine graphene) system. (a) The continuum model for the system with a hollow-ball interacting with a plate. (b) MD model for the system.

Note 5. Polar coordinate system and specific atomic positions in graphene sheets

Taking the graphene sheet with $C_6(3)$ grain boundaries (GBs) as an example, $r-\theta$ polar coordinate system is constructed in **Fig. S4**. Six atoms are chosen in the coordinate system. Their coordinate positions are atom-a $(r,\theta)=(30,0)$, atom-b $(r,\theta)=(45,0)$, atom-c $(r,\theta)=(30,\pi/4)$, atom-d $(r,\theta)=(45,\pi/4)$, atom-e $(r,\theta)=(30,\pi/2)$ and atom-f $(r,\theta)=(45,\pi/2)$, respectively.
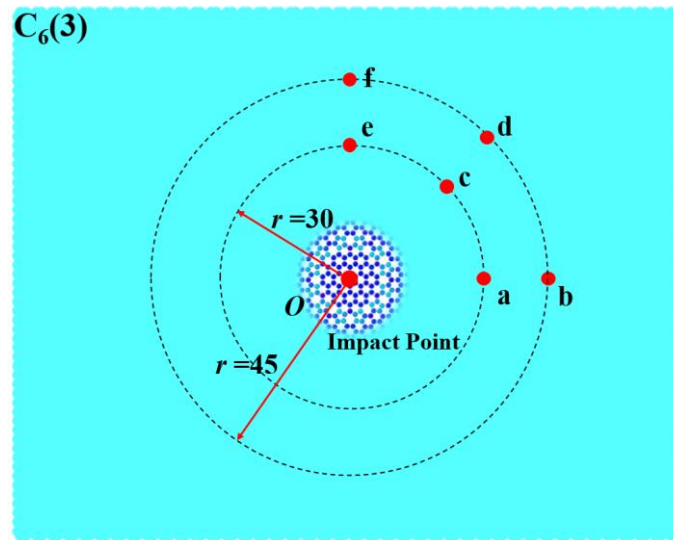
Fig. S4. Polar coordinate system (r,θ) is constructed in the graphene sheet with $C_6(3)$ GBs. The impact point is at original point O in the polar coordinate. Atom-a to atom-f are defined in the coordinate system. The atomic coordinates are atom-a $(r,\theta)=(30,0)$, atom-b $(r,\theta)=(45,0)$, atom-c $(r,\theta)=(30,\pi/4)$, atom-d $(r,\theta)=(45,\pi/4)$, atom-e $(r,\theta)=(30,\pi/2)$ and atom-f $(r,\theta)=(45,\pi/2)$, respectively.

Note 6. Variations of specific atomic x- and y-coordinate for atoms in the $(r,\pi/4)$ axis

As shown in **Figs. S5**a-d, the evolutions for specific atomic x- and y-coordinate of atom-c $(r,\theta)=(30,\pi/4)$ and atom-d $(r,\theta)=(45,\pi/4)$ in terms of time are plotted. The moderate atomic fluctuation can be found in the figures.
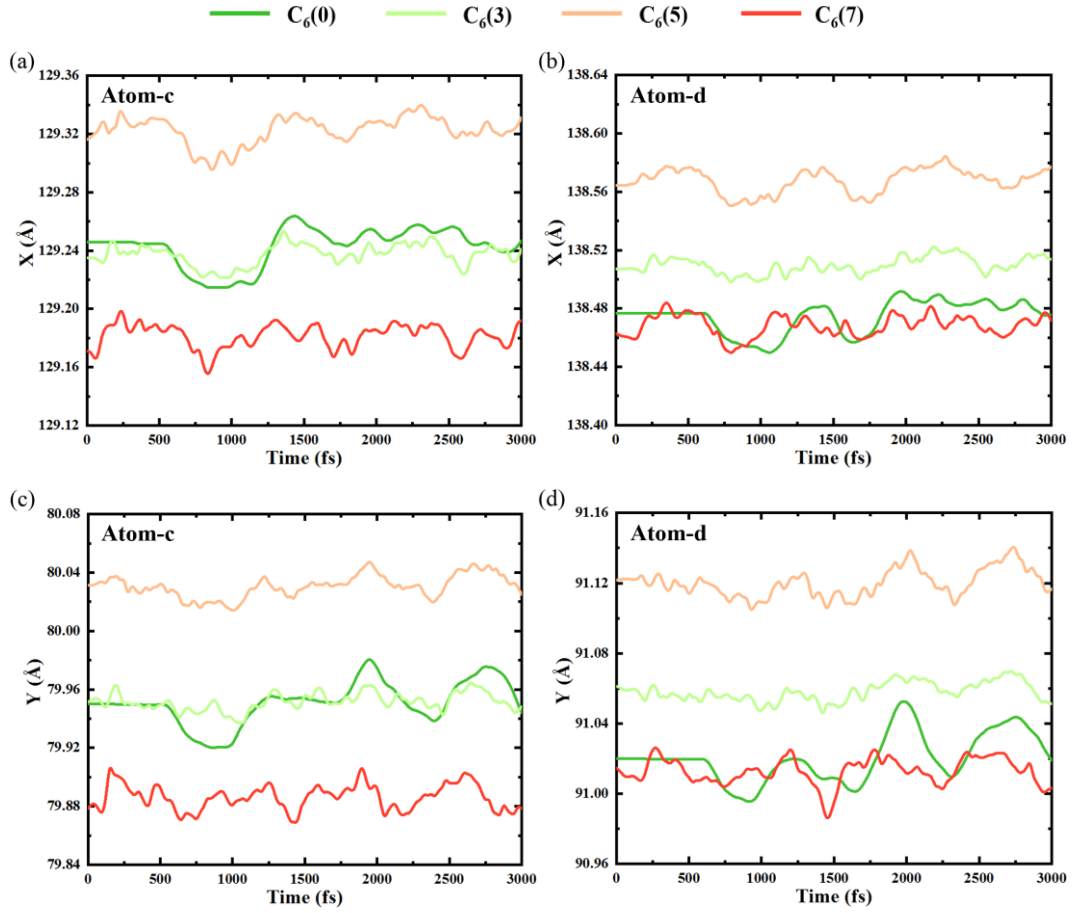

Fig. S5. Variations for x-coordinate of (a) atom-c $(r,\theta)=(30,\pi/4)$, (b) atom-d $(r,\theta)=(45,\pi/4)$ and y-coordinate of (c) atom-c $(r,\theta)=(30,\pi/4)$, (d) atom-d $(r,\theta)=(45,\pi/4)$. The coordinate is in the unit of Å.

Note 7. Variations of specific atomic strain energy for atoms in the $(r,\pi/4)$ axis

Fig. S6 presents the evolutions of the specific atomic strain energy for atom-c $(r,\theta)=(30,\pi/4)$ and atom-d $(r,\theta)=(45,\pi/4)$ with respect to time. The specific atomic strain energies increase significantly for the defective graphene sheets. However, the moderate atomic fluctuation occurs in pristine graphene.
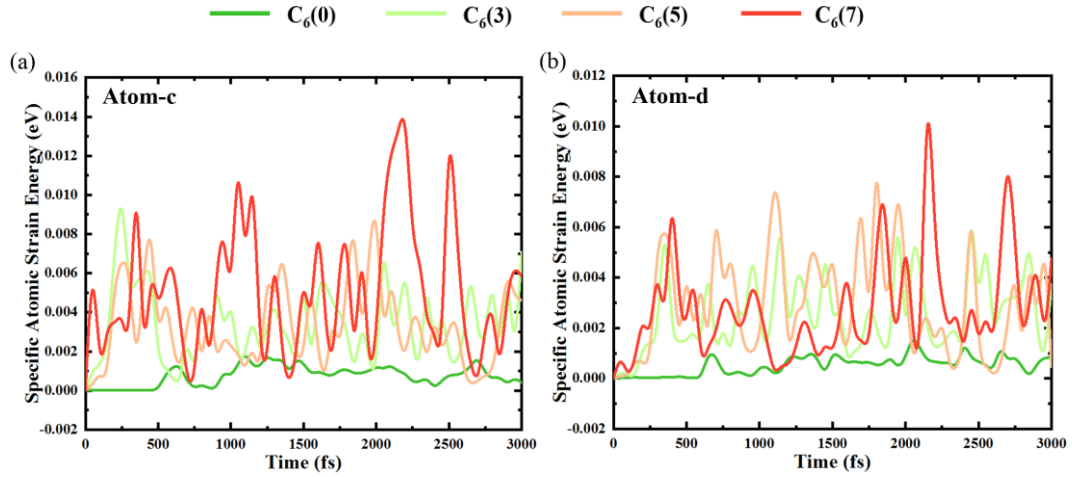

Fig. S6. Variations for specific atomic strain energy of (a) atom-c $(r,\theta)=(30,\pi/4)$, (b) atom-d $(r,\theta)=(45,\pi/4)$. The energy is in the unit of eV.

Note 8. Evolution of van der Waals (vdW) potential energy for the graphene sheets

Fig. S7 depicts the evolution of the vdW potential energy in terms of time for the four graphene sheets (i.e., pristine graphene and the graphene sheets with $C_6(3)$, $C_6(5)$ and $C_6(7)$ GBs). The red arrows denote the evolution trends of the vdW potential energy for the graphene sheets. The curves indicate the vdW potential energy exist only during the interaction phase.
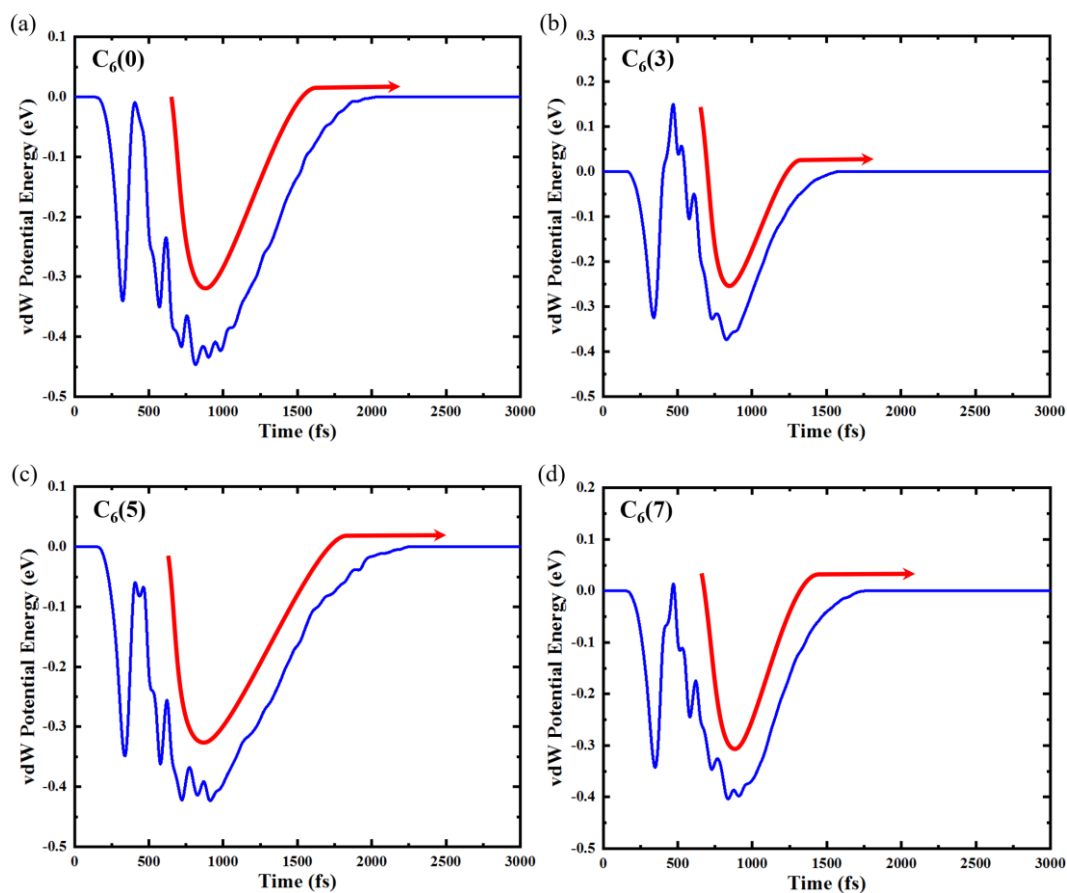

Fig. S7. The evolution of the vdW potential energy in terms of time for (a) pristine graphene and the graphene sheets with (b) $C_6(3)$ GBs, (c) $C_6(5)$ GBs, (d) $C_6(7)$ GBs. The energy is in the unit of eV.

Note 9. Effects of initial velocity and temperature variation on the out-of-plane displacement along the (*r*,0) and (*r*,π/2) axes

Figs. S8a-h describe the effects of different initial velocities (15 Å/ps, 30 Å/ps, 45 Å/ps and 60 Å/ps) and temperature variations (5 K, 25 K, 50 K, 75 K and 100 K) on the out-of-plane displacement (Δz) for pristine graphene and the graphene sheet with $C_6(7)$ GBs along the axes (*r*,0) and (*r*,π/2). "V" shape (see 15 Å/ps in **Fig. S8**a) and "W" shape (see **Fig. S8**b) can be observed. The results indicate that the higher velocity (larger than 15 Å/ps, such as 45 Å/ps) and temperature (such as 75 K and 100 K) can accelerate the transformation of the potential energy for graphene sheet into its kinetic energy and dynamic wrinkling propagation.
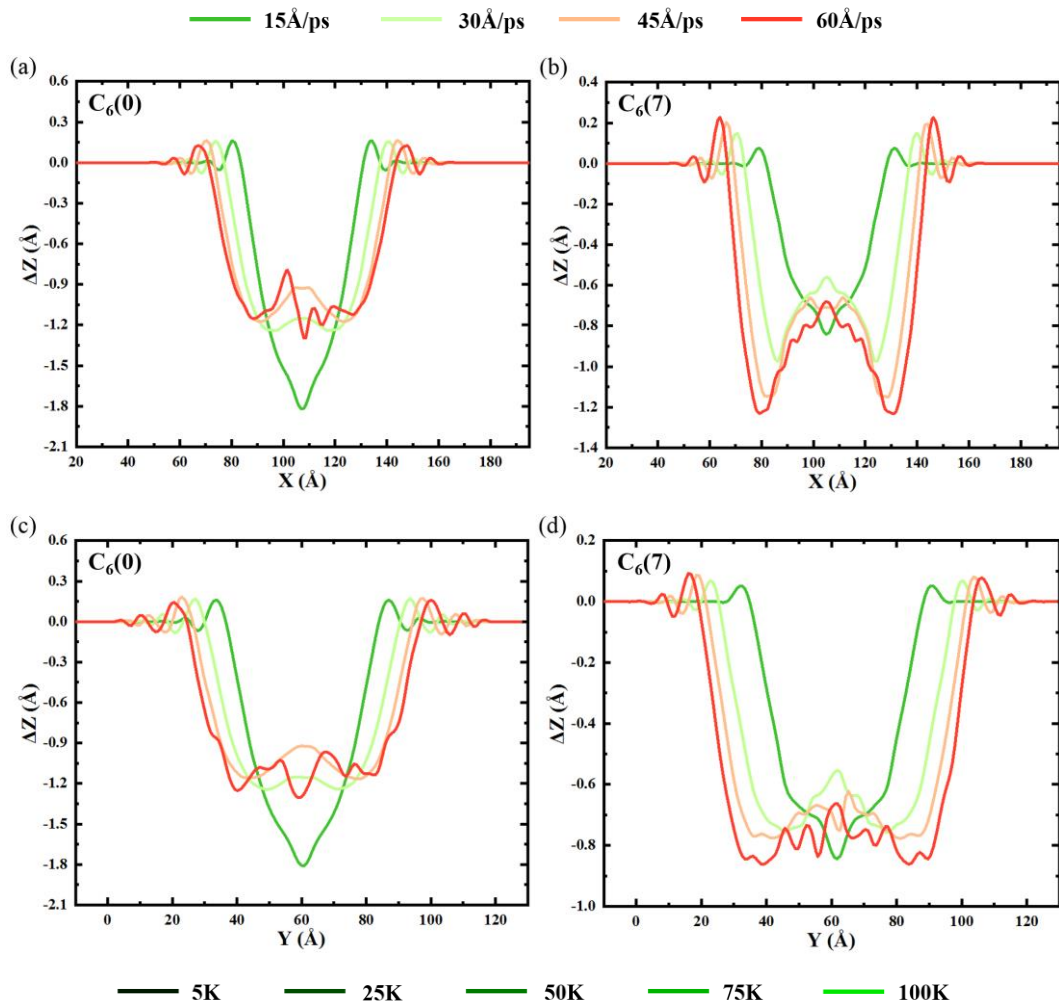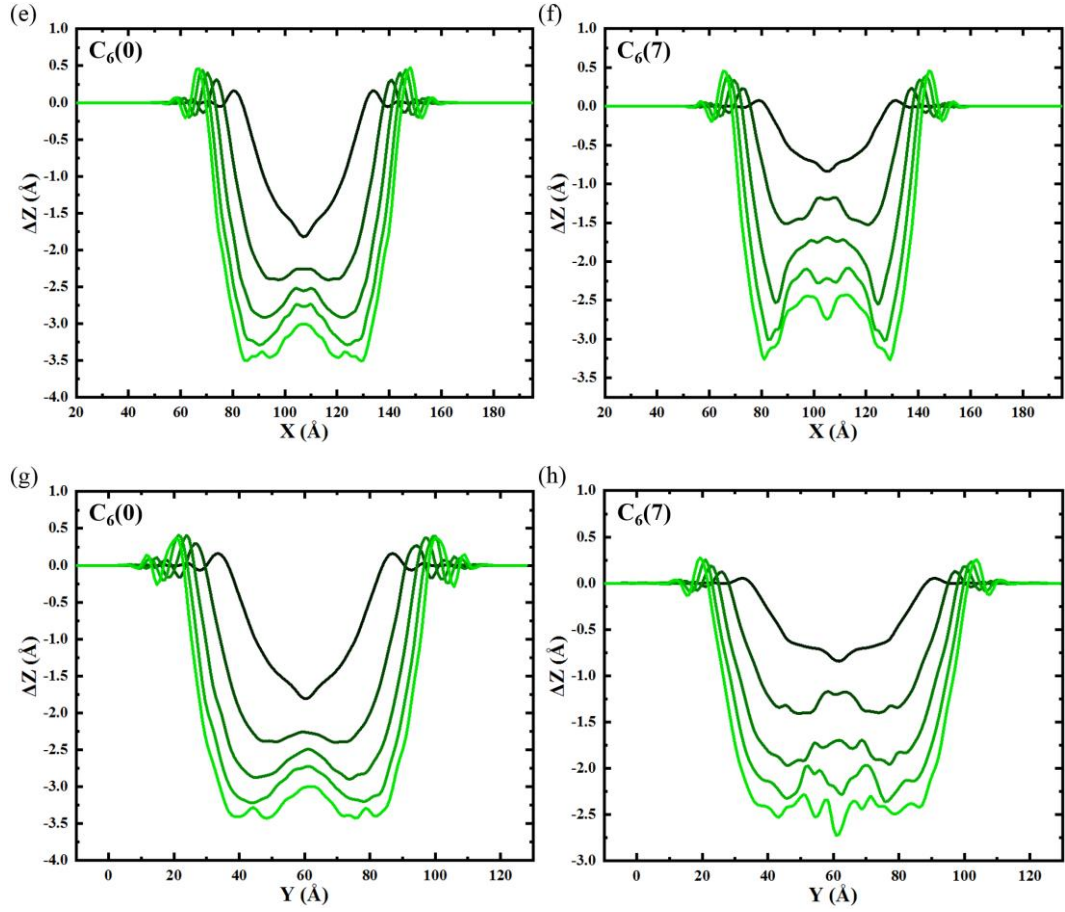
Fig. S8. The curves of the out-of-plane displacement (Δz) along the axes (r,0) and (r,π/4) with different initial velocities (15 Å/ps, 30 Å/ps, 45 Å/ps and 60 Å/ps) and temperature variations (5 K, 25 K, 50 K, 75 K and 100 K) at 1000 fs. (a)-(d) show the out-of-plane displacement (Δz) along the axes (r,0) and (r,π/4) for pristine graphene and the graphene sheet with C_6(7) GBs at different initial velocity. (e)-(h) show the out-of-plane displacement (Δz) along the axes (r,0) and (r,π/4) for pristine graphene and the graphene sheet with C_6(7) GBs at different temperature variation. The displacement is in the unit of Å.

Note 10. Wrinkle propagation in the graphene sheets with point and Stone Wales (SW) defects

As shown in **Fig. S9**, molecular dynamics (MD) simulations are performed to study wrinkle propagation in the graphene sheets with point defect and single SW defect. The figures reveal the distributions of the out-of-plane displacement field, z-direction velocity, instantaneous atomic kinetic energy and instantaneous atomic strain energy in the graphene sheets with point defect (see **Fig. S9**a) and SW defect (see **Fig. S9**b). The distinctly different contours of dynamic wrinkling propagation can be observed at 1250 fs. The results indicate the ability of dynamic wrinkle propagation for defect detection.
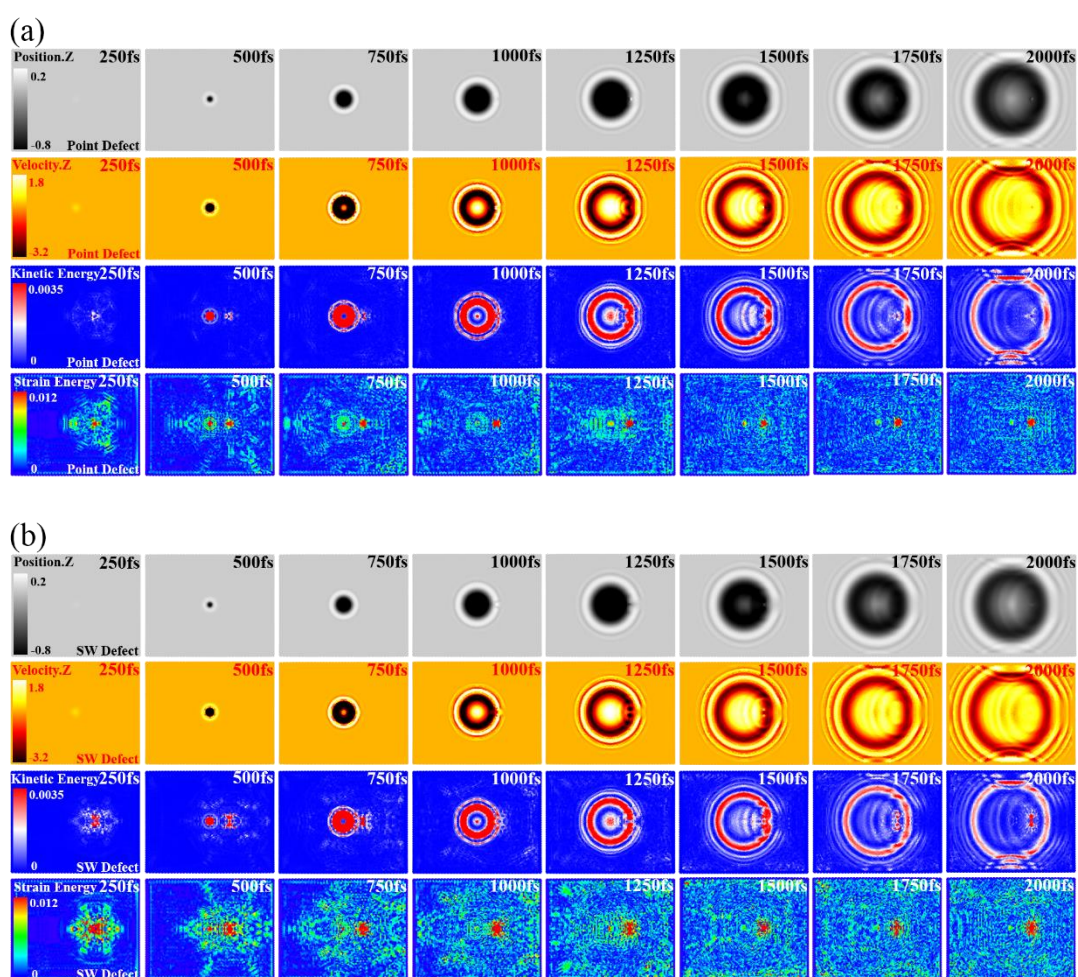

Fig. S9. MD simulation results of the graphene sheets with point defect and SW defect induced by C60 molecule. The distributions of the out-of-plane displacement field, z-direction velocity, instantaneous atomic kinetic energy and instantaneous atomic strain energy in the graphene sheets with (a) point defect and (b) SW defect. The units of displacement, velocity and energy are Å, Å/ps and eV, respectively.

Note 11. Evolution of various energies for the graphene sheets with external excitation

Figs. S10a-j reveal the evolution of the specific atomic strain energy for atom-a and atom-b (see **Figs. S10**a-b), the total potential energy increment for the four graphene sheets (see **Figs. S10**c-f) and the vdW potential energy between C60 molecule and graphene sheet (see **Figs. S10**g-j) with external excitation (i.e., the impact point is outside the GBs). With the time increasing, the specific atomic strain energies of atom-a and atom-b for pristine graphene show the moderate variation. Additionally, two evolution modes of the total potential energy increment (see **Figs. S10**c-f) can be observed. As shown in **Figs. S10**c-f, the red arrows present the evolution trends of the vdW potential energy. The curves of the vdW potential energy indicate the vdW potential energy exist before 3000 fs.
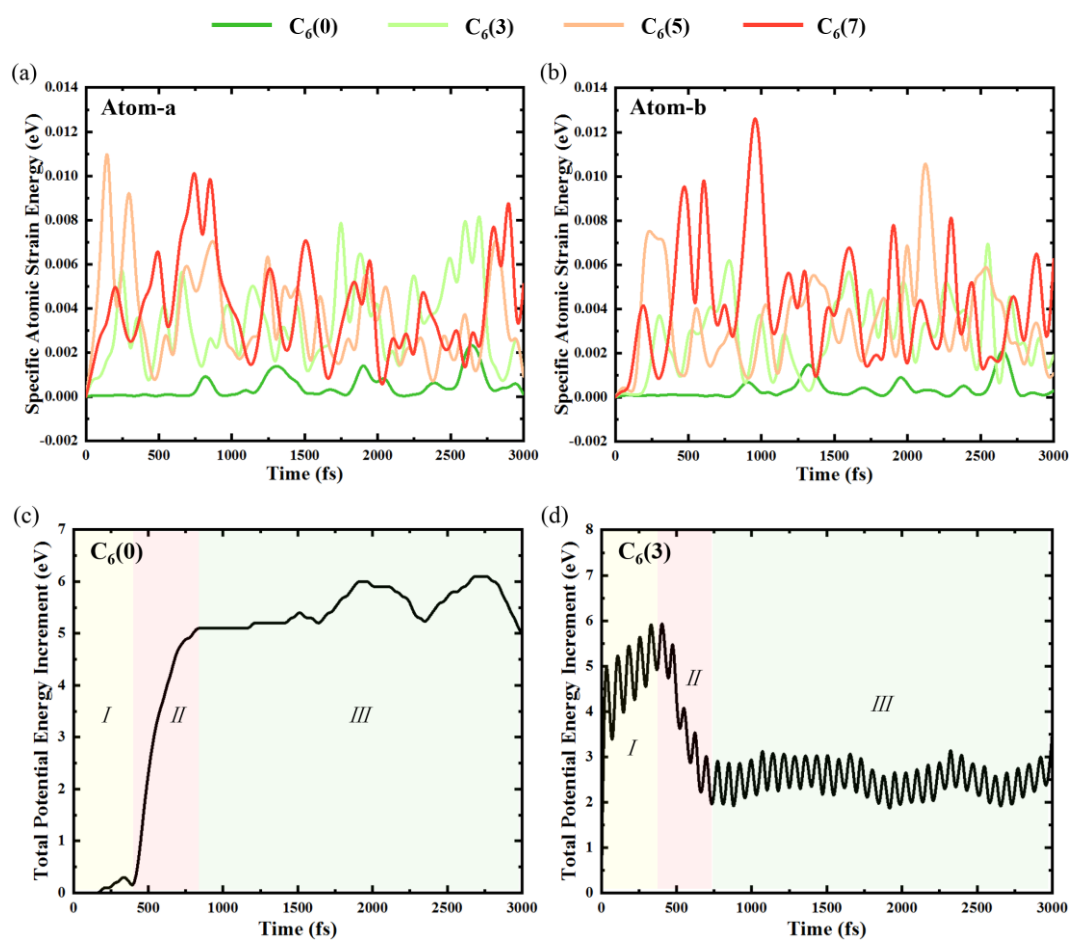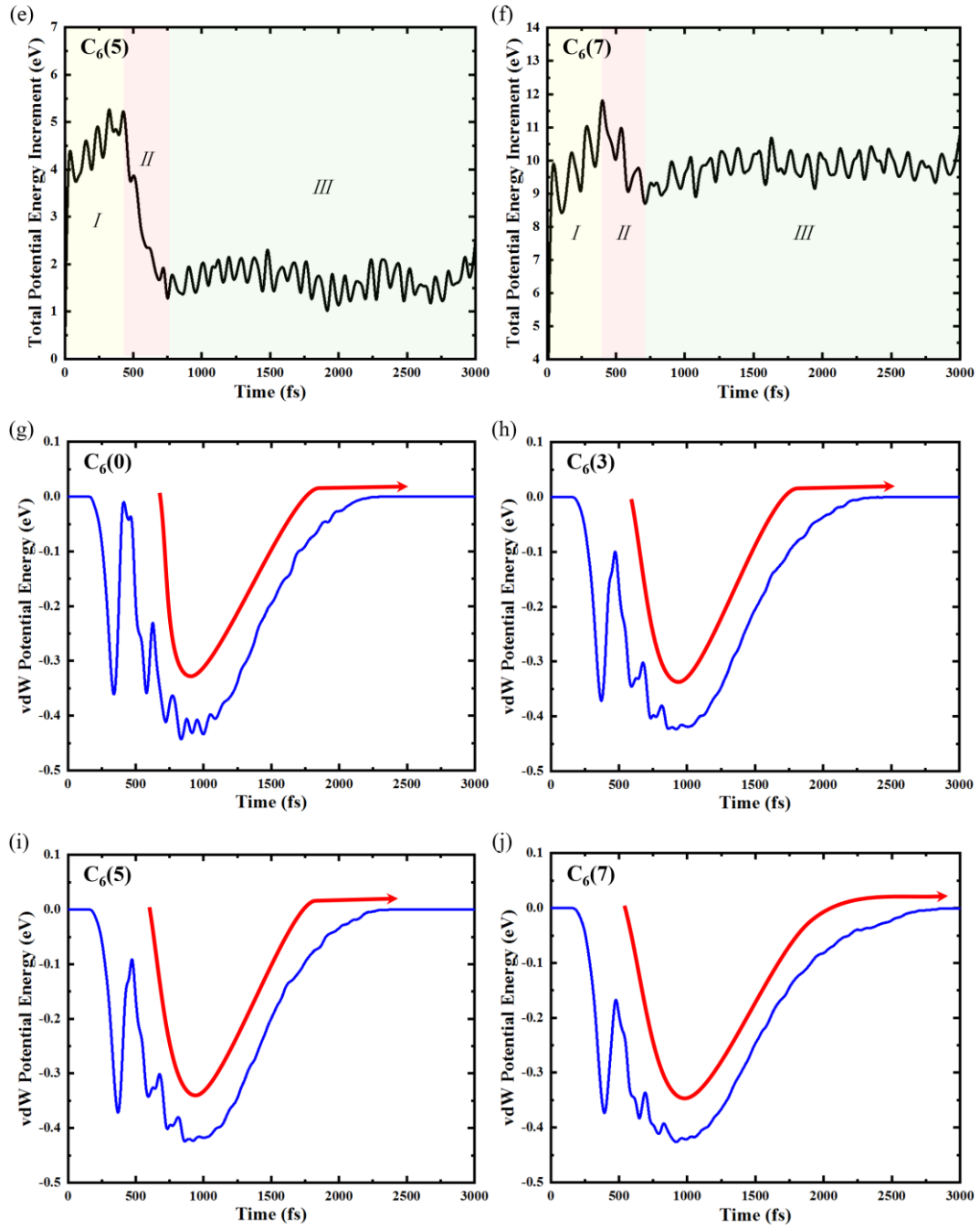
Fig. S10. Evolution of various energies for the graphene sheets induced by external excitation. Specific atomic strain energies for (a) atom-a $(r,\theta)=(30,0)$ and (b) atom-b $(r,\theta)=(45,0)$. Total potential energy increments for (c) pristine graphene and the graphene sheets with (d) $C_6(3)$ GBs, (e) $C_6(5)$ GBs, (f) $C_6(7)$ GBs. vdW potential energies for (g) pristine graphene and the graphene sheets with (h) $C_6(3)$ GBs, (i) $C_6(5)$ GBs, (j) $C_6(7)$ GBs. The energy is in the unit of eV.

Note 12. Out-of-plane displacements of the graphene sheets at different time with external excitation

The out-of-plane displacements along the $(r,0)$ axis at different time (1200 fs, 1800 fs, 2400 fs, 3000 fs and 3300 fs) are plotted, as shown in **Figs. S11**a-d. In the same graphene sheet, the amplitude of the dynamic wrinkle decreases with the time evolution. The relationship of the minimum amplitude (see 3300 fs) for the out-of-plane displacement is $C_6(0)>C_6(5)>C_6(3)>C_6(7)$.
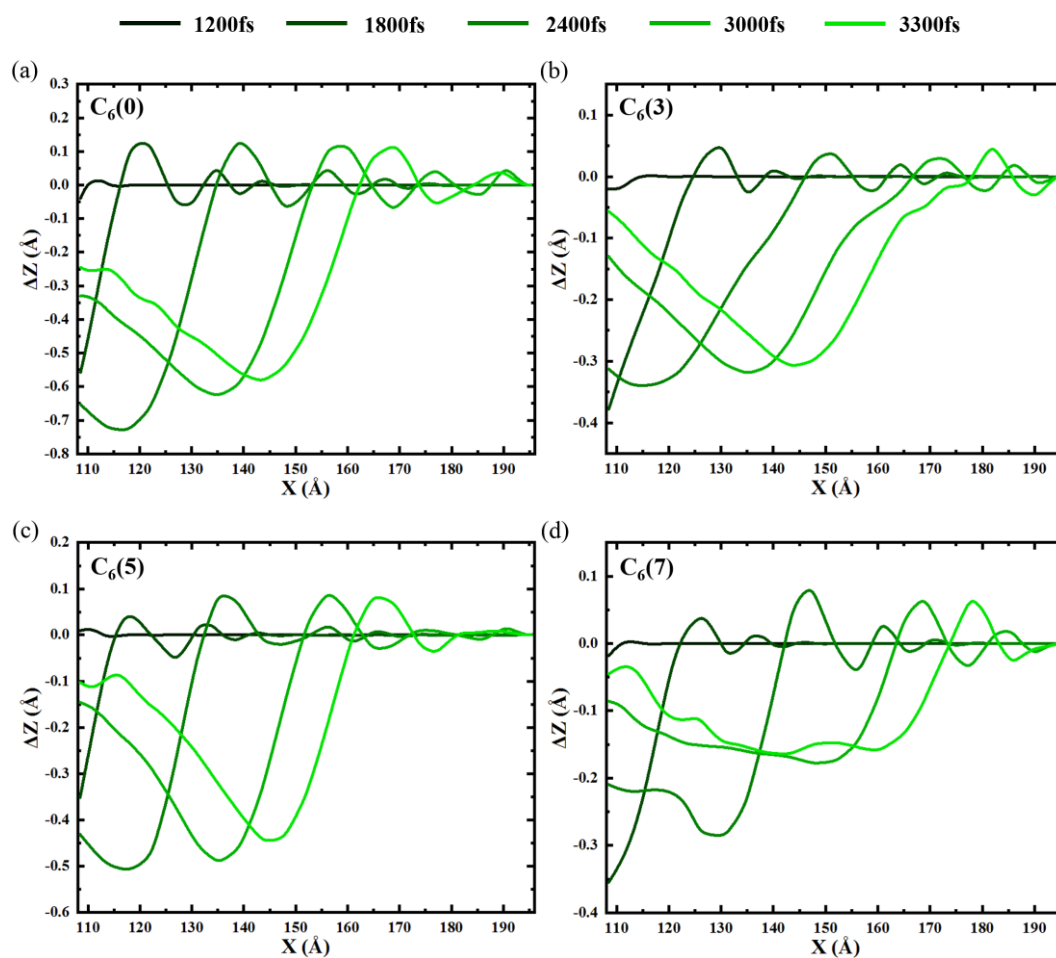

Fig. S11. The out-of-plane displacements along the $(r,0)$ axis at different time (1200 fs, 1800 fs, 2400 fs, 3000 fs and 3300 fs). (a)-(d) show the out-of-plane displacements for pristine graphene and the graphene sheets with $C_6(3)$, $C_6(5)$ and $C_6(7)$ GBs.

Reference

1 E. Cockayne, G. M. Rutter, N. P. Guisinger, J. N. Crain, P. N. First and J. A. Stroscio, Grain boundary loops in graphene, *Phys. Rev. B*, 2011, **83**(19), 195425.

2 S. J. Stuart, A. B. Tutein and J. A. Harrison, A reactive potential for hydrocarbons with intermolecular interactions, *J. Chem. Phys.*, 2000, **112**(14), 6472-6486.

3 D. Brenner, O. Shenderova, J. Harrison, S. Stuart, B. Ni and S. Sinnott, A second-generation reactive empirical bond order (REBO) potential energy expression for hydrocarbons, *J. Phys. Condens. Matter*, 2002, **14**(4), 783-802.

4 J. Wu, H. Zhao, J. Liu, Z. Zhang, F. Ning and Y. Liu, Nanotube-chirality-controlled tensile characteristics in coiled carbon metastructures, *Carbon*, 2018, **133**, 335-349.

5 J. Tersoff, New empirical approach for the structure and energy of covalent systems, *Phys. Rev. B*, 1988, **37**(12), 6991-7000.

6 F. Pavia and W. A. Curtin, Interfacial sliding in carbon nanotube/diamond matrix composites, *Acta Mater.*, 2011, **59**(17), 6700-6709.

7 S. Hosseini Hashemi, A. Sepahi Boroujeni and S. Sepahi-Boroujeni, Analytical and molecular dynamics studies on the impact loading of single-layered graphene sheet by fullerene, *Appl. Surf. Sci.*, 2018, **437**, 366-374.

8 S. Hosseini Hashemi and A. Sepahi Boroujeni, Elastic impact response of a nonlocal rectangular plate, *Int. J. Solids Struct.*, 2017, **109**, 93-100.

9 S. C. Pradhan and J. K. Phadikar, Small scale effect on vibration of embedded multilayered graphene sheets based on nonlocal continuum models, *Phys. Lett. A*, 2009, **373**(11), 1062-1069.

10 Y. Chan and J. M. Hill, Modelling interaction of atoms and ions with graphene, *Micro & Nano Letters*, 2010, **5**(5).

11 T. A. Hilder and J. M. Hill, Theoretical comparison of nanotube materials for drug delivery, *Micro & Nano Letters*, 2008, **3**(1).